

UNCLASSIFIED

SECURITY CLASSIFICATION OF THIS PAGE (When Data Entered)

REPORT DOCUMENTATION PAGE

READ INSTRUCTIONS BEFORE COMPLETING FORM

1. REPORT NUMBER ② Memorandum Rept.	2. GOVT ACCESSION NO.	3. RECIPIENT'S CATALOG NUMBER
4. TITLE (and Subtitle) Speed and Depth Effects in Magnetic Anomaly Detection	5. TYPE OF REPORT & PERIOD COVERED	
6. AUTHOR(s) Edward P. Loane	6. PERFORMING ORG. REPORT NUMBER	
9. PERFORMING ORGANIZATION NAME AND ADDRESS EPL Analysis Ashton, MD 20702	10. PROGRAM ELEMENT, PROJECT, TASK AREA & WORK UNIT NUMBERS	
11. CONTROLLING OFFICE NAME AND ADDRESS CNO(OP-96) Washington, D.C. 20350	12. REPORT DATE 12 October 1976	13. NUMBER OF PAGES 30
14. MONITORING AGENCY NAME & ADDRESS (if different from Controlling Office) 1231	15. SECURITY CLASS. (of this report) Unclassified	
16. DISTRIBUTION STATEMENT (of this Report) Unlimited and approved for Public release.		
17. DISTRIBUTION STATEMENT (of the abstract entered in Block 20, if different from Report)		
18. SUPPLEMENTARY NOTES		
19. KEY WORDS (Continue on reverse side if necessary and identify by block number) Advanced Naval Vehicle Concepts Evaluation ANVCE Military Worth Total Field Magnetometer Speed and Depth (or Altitude)		
20. ABSTRACT (Continue on reverse side if necessary and identify by block number) This memorandum presents a theoretical evaluation of the effects of speed and depth (or altitude) on the ASW detection performance of a total field magnetometer. Median or nominal detection ranges are calculated for alternative sensor speeds, sensor depths, and criteria for detection.		

ADA 081 329

DDC FILE COPY

DTIC
SELECTED
FEB 28 1980

409403

18

gp 5004L

EPL Analysis

CONSULTANTS IN
APPLIED MATHEMATICS, OPERATIONS RESEARCH

EDWARD P. LOANE
PETER S. SHOENFELD

17800 EDNOR VIEW TERRACE
ASHTON, MD. 20702
(301) 924-3574

October 12, 1976

To: Advanced Naval Vehicle Concept Evaluation Study
Office of the Chief of Naval Operations (OP-96V)

From: Edward P. Loane

Subject: Speed and Depth Effects in Magnetic Anomaly
Detection

This memorandum presents a theoretical evaluation of the effects of speed and depth (or altitude) on the ASW detection performance of a total field magnetometer. Median or nominal detection ranges are calculated for alternative sensor speeds, sensor depths, and criteria for detection; the principal results are displayed in Table 1 of the following section. The calculated results are intended to be neither pessimistic nor optimistic, but to be best estimates supported by available background noise data. It should be noted that the relevant detection parameter depends on the inverse fifth or sixth power of range, vice signal or noise power with exponent one; whence changes of a signal or noise power by a factor of ten result in at most a 50% increase or decrease in detection range.

Accession for	
NIS	SEARCHED
DOC	TAB
Unannounced	
Justification	
By _____	
Date _____	
Availability Codes	
Dist	Avail and/or special
A	

SEARCHED
SERIALIZED
INDEXED
OCT 15 1976

DISTRIBUTION STATEMENT A
Approved for public release;
Distribution Unlimited

80 2 27 139

Summary.

The principal calculated results of the present analysis are shown in Table 1 and discussed in this section. A qualitative description of the effects of speed and depth on magnetometer detection performance is given first, followed by a list of the assumptions embodied in the calculated values shown. The limitations of this analysis are noted at the end of the section.

The effects of sensor speed and depth on magnetic anomaly detection performance are explained, qualitatively, as follows. First, the time-varying signal by which an anomaly is detected is generated largely by the search vehicle's own motion. For a given CPA, a slower search speed results in an elongated (i.e., lower frequency content) signal which is generally disadvantageous since geomagnetic background noise levels increase with decreasing frequency. This is portrayed, quantitatively in Figures 6 and 8 of the second and third sections. Second, at or near the ocean surface, background noise levels are dominated by ocean wave noise, i.e., a time-varying magnetic field produced by the motion of sea water in the earth's field. Ocean wave noise levels decay rapidly with sensor altitude (and less rapidly with depth below the surface) so that at altitudes of 500 ft. (or somewhat greater depth) other sources of background noise predominate. Finally, as a complicating factor, power spectra of some components of background noise are affected by search speed, via Doppler shift of ocean wave noise and the actual generation of geologic noise (due to magnetic anomalies in the earth's crust). In the present analysis, geologic noise is negligible; where ocean wave noise is significant, vehicle speed is advantageous by shifting noise power to frequencies greater than those relevant to detection.

TABLE 1

CALCULATED MAGNETIC ANOMALY DETECTION RANGES
(Slant Range)

Notes: (1) The two numbers shown for each case are based on differing criteria for detection. The first, modeling current capabilities, assumes a signal is detectable if and only if its amplitude is three times the background noise level; the second represents optimal signal processing performance in the presence of (assumed) Gaussian background noise.

(2) Inputs and assumptions supporting the calculated values are listed in the text.

(3) It is conjectured that ocean wave noise levels are understated at lower wind speeds for reasons given in the text. Even at zero current wind speeds long period ocean waves and, hence, magnetic noise may approach values calculated for 30 knot winds, whence detection ranges for a 30 knot wind would also pertain.

Sensor Depth and Surface Wind Speed (Governing ocean-wave noise)	Platform Speed		
	30 knot	60 knot	120 knot
Negligible Ocean Wave Noise (Sensor above 500 ft. altitude or below 500 ft. depth with surface winds below 20 kt.) (See Note 3)	910 ft.	1050 ft.	1140 ft.
	1230 ft.	1440 ft.	1550 ft.
Sensor at 500 ft. depth with 30 kt. surface winds	870 ft.	990 ft.	1060 ft.
	1100 ft.	1330 ft.	1410 ft.
Sensor within 50 ft. of surface with 20 knot surface winds (See Note 3)	800 ft.	910 ft.	970 ft.
	1080 ft.	1290 ft.	1370 ft.
Sensor within 50 ft. of surface with 30 knot surface winds	610 ft.	630 ft.	650 ft.
	820 ft.	880 ft.	900 ft.

Because of the important frequency effects in background noise levels, extrapolation of operational performance with high speed (e.g., 300 knot) platforms to the lower speeds considered in the present analysis is erroneous; further, noise levels quoted for high speed platforms are inappropriate in the present context. This has necessitated the detailed but theoretical approach of the present memorandum, for which, unfortunately, measured values of the required inputs are sparse and not in good agreement.

The particular assumptions embodied in the calculated values of Table 1 are summarized as follows:

- (i) Target submarine magnetic moment of $7.5 \cdot 10^8 \gamma/3$ ft.
- (ii) Most favorable detection geometry (i.e., orientation of earth's magnetic field, target moment, relative velocity and searcher/target vector at CPA).
- (iii) Relative speed equal to sensor search speed.
- (iv) Geomagnetic noise power spectrum as given by Figure 6 (a summary of measured values).
- (v) Ocean wave noise power spectra as given by Figure 5 (a theoretical calculation based on the stationary Pierson-Moskowitz spectrum of mean square ocean wave height as a function of wind speed).
- (vi) Search vehicle track random with respect to wind direction and, hence, direction of wave motion.
- (vii) Negligible geologic magnetic noise.
- (viii) Negligible platform specific background noise.
- (ix) Current detection capabilities modeled by the criterion - detection if and only if the magnetic anomaly signal is three times background noise level. In implementing this criterion, signal and noise levels are derived from corresponding powers in an optimally chosen frequency band.

- (x) Optimal signal processing capability given by matched filter detection of a known signal in Gaussian noise (i.e., Anderson function matching); a false alarm rate of .5/hour is fixed for calculating probabilities of detection.

All of these assumptions are discussed in a quantitative fashion in following sections which treat, respectively, the signal, the noise background, and the detection of signal in noise.

There are three significant uncertainties in the calculation of detection ranges displayed in Table 1 which are discussed below.

First, an appropriate value for the target submarine's magnetic moment is largely conjectural, with the correct value depending primarily on the submarine displacement, previous history of motion in the earth's magnetic field and degaussing attempts. Aside from degaussing, the effects on calculated detection range would be minimal, however, current degaussing techniques can reduce the submarine's magnetic moment by greater than a factor of ten (signal energy at a given CPA by a factor of 100) which would result in significant reductions in detection range.

Second, the theoretical calculation of ocean wave noise levels and power spectra for wind speeds below 30 knots is suspect. The calculation is based on the stationary Pierson-Moskowitz r.m.s. wave height spectrum, which, for low wind speeds predicts no long period (e.g., 10-12 second) ocean waves. Such long period waves are the principal contributors to magnetic noise at the surface and at depth, and are present in the open ocean even when the current surface winds are low.

Finally, the detection criterion - detection if and only if the signal is three times the background noise level - is based on empirical tests from high speed platforms. At lower speeds, the relevant background noise frequency dependence is different, and the signal is considerably distorted due to truncation of low frequency components, whence this criterion may no longer be appropriate.

Magnetic Anomaly Signal.

Representing the target submarine by a magnetic dipole moment, the target's magnetic field at the sensor is given by

$$\vec{B} = \frac{-1}{r^3} \left[\vec{m} - \frac{3(\vec{m} \cdot \vec{r})\vec{r}}{r^2} \right] \quad (1)$$

where

- \vec{B} = the (vector) magnetic field at the sensor,
- \vec{m} = the (vector) dipole moment representing the submarine,
- \vec{r} = the vector from the sensor to the target, and
- $r = |\vec{r}|$, i.e., the slant range.

A total field magnetometer responds to the sum of this anomaly and the earth's field; the latter field dominates (by several orders of magnitude) whence the magnitude of the total field at the sensor is given by

$$B_T = B_E + (\vec{I}_E \cdot \vec{B}) \quad (2)$$

where

- B_T = the magnitude of the total field measured,
- B_E = the magnitude of the earth's field at the sensor, and
- \vec{I}_E = a unit vector giving the direction of the earth's field at the sensor.

The earth's field is sensibly constant over the duration of an encounter, whence the constant term in formula (2) is filtered out, leaving a time-varying signal given by the dot product of \vec{I}_E and the right-hand side of equation (1) (time variations in the earth's field are treated in the next section).

Finally, assuming both the target and sensor move along straight tracks so that, as a function of time t ,

$$\vec{r}(t) = \vec{V}t + \vec{r}_0 \quad (3)$$

(here $t = 0$ corresponds to CPA), the time-varying signal is given by

$$B_D(t) = \frac{m}{r_0^3} \left[\frac{A_1}{\left((Vt/r_0)^2 + 1 \right)^{5/2}} + \frac{A_2(Vt/r_0)}{\left((Vt/r_0)^2 + 1 \right)^{5/2}} + \frac{A_3(Vt/r_0)^2}{\left((Vt/r_0)^2 + 1 \right)^{5/2}} \right] \quad (4)$$

where

- B_D = the magnitude of the time-varying field,
- V = the sensor/target relative speed,
- r_0 = the distance at CPA, and
- A_1, A_2 and A_3 = scalar coefficients described below.

The functions

$$\phi_i \left(\frac{Vt}{r_0} \right) = \frac{(Vt/r_0)^{i-1}}{\left((Vt/r_0)^2 + 1 \right)^{5/2}} \quad \text{for } i = 1, 2, 3$$

are known as Anderson functions, and are displayed, along with their corresponding Fourier spectra, in Figures 1 and 2. The presentation of Figure 1 employs the dimensionless parameter

$$\theta = \frac{Vt}{r_0}$$

whence the spectra are plotted in terms of the dimensionless quantity

FIGURE 1

ANDERSON FUNCTIONS, $\phi_1(\theta)$

Note differences in vertical scales.

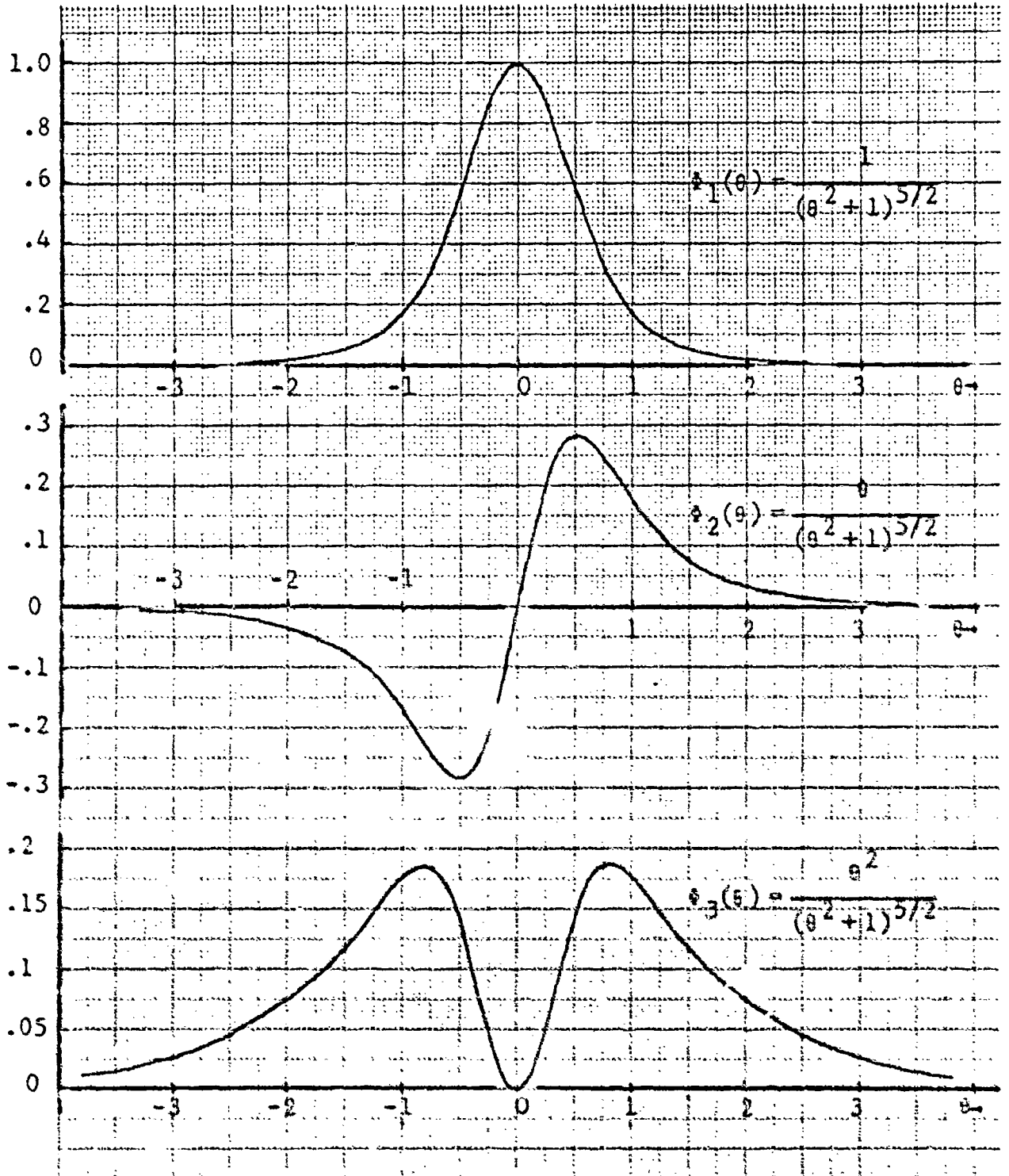


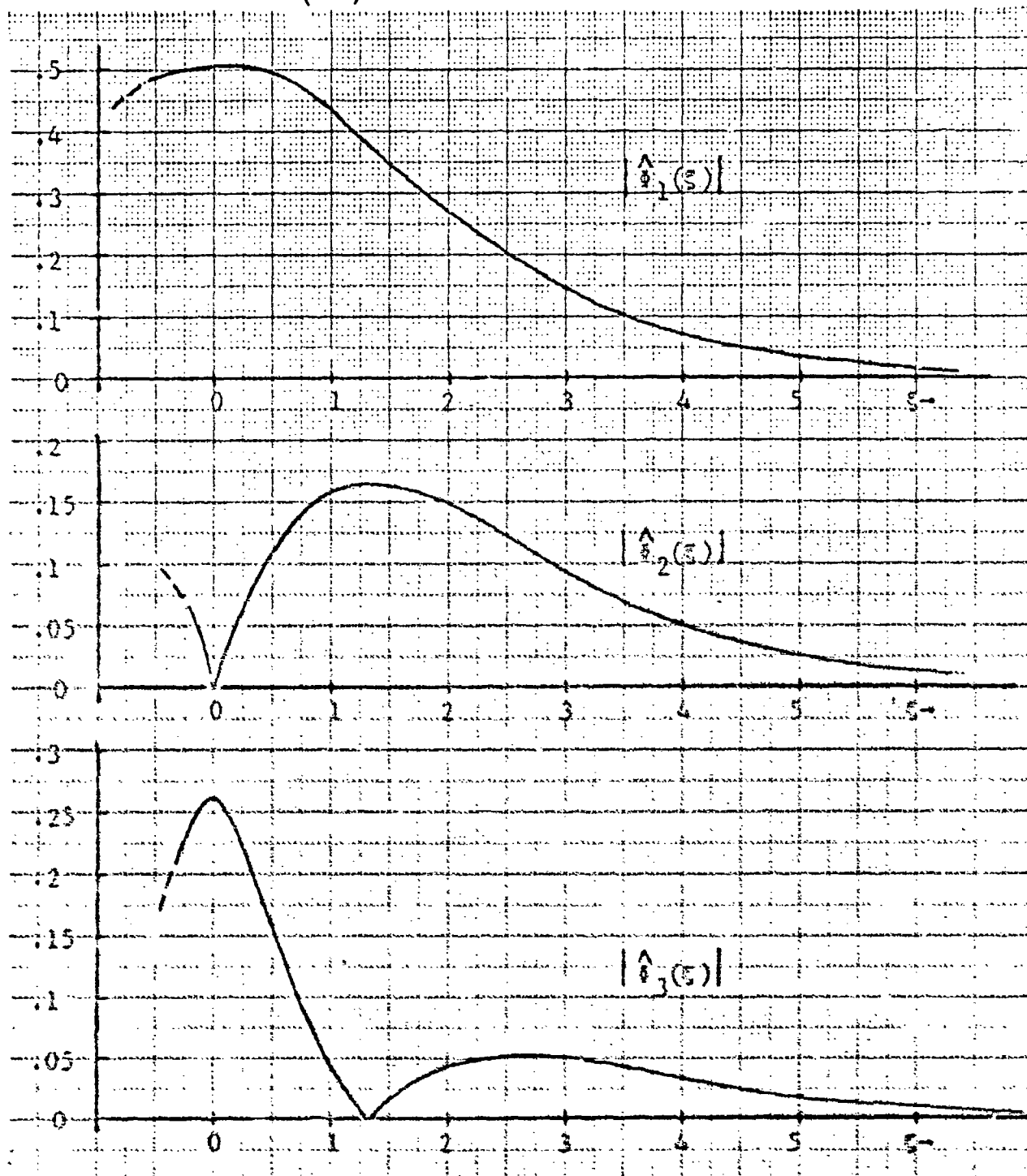
FIGURE 2

ABSOLUTE VALUE OF FOURIER SPECTRA OF ANDERSON FUNCTIONS

Notes: (1) $|\hat{\phi}_i(\xi)| = \left| \frac{1}{\sqrt{2\pi}} \int_{-\infty}^{\infty} \phi_i(\theta) e^{-i\theta\xi} d\theta \right|$.

$|\hat{\phi}_i|$ is symmetric about $\xi = 0$.

(2) For a time varying signal given by $\phi_i(Vt/r_0)$ the absolute value of the Fourier transform is given by $\frac{r_0}{V} |\hat{\phi}_i(\frac{w r_0}{V})|$ where $w = 2\pi$ [frequency].



$$\xi = \frac{r_0^w}{V}$$

which is the Fourier dual of Vt/r_0 .

The coefficients A_1 , A_2 and A_3 are sums of dot products of unit vectors specifying the orientation of the earth's field, the submarine moment, the direction of relative motion and the sensor/target direction of CPA; basically, these define the geometry of the encounter. It is not the purpose of this memorandum to treat various geometries in detail, hence some simplifications are employed. The coefficients can be bounded by

$$|A_1|, |A_3| \leq 2 \cos \alpha \sim 1.0$$

$$|A_2| \leq 3 \cos \alpha \sim 1.5$$

where α is the declination of the earth's magnetic field, here taken to be 60° . In the subsequent calculations of detection performance, the Anderson functions are treated separately with detectability or detection range taken to be the maximum of that attained for the three possibilities. Further, the value assumed for the target submarine magnetic moment, m , in subsequent calculation is

$$m = 7.5 \cdot 10^8 \text{ } \gamma/\text{ft}^3.$$

Noise Background.

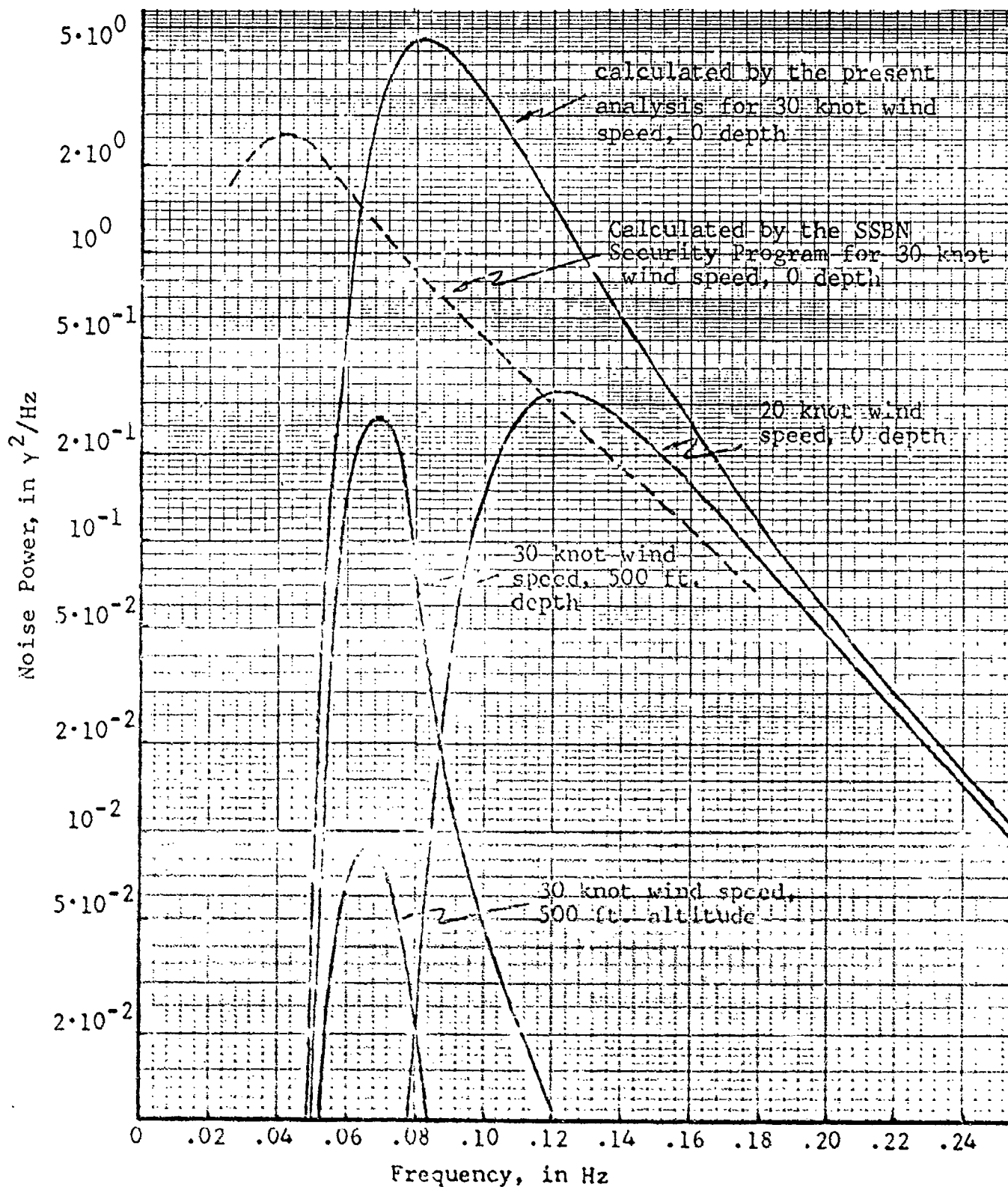
The magnetic noise background at the sensor is composed of environmental noise and platform specific noise. Platform specific noise, including vehicle noise, translational noise and internal noise of the sensor, is ignored in the present analysis as it does not appear to limit detection performance. If the sensor is employed at the ocean surface, ocean wave noise dominates the background; if the sensor is towed at sufficient depth so that wave noise is not important (e.g., 500 ft.) then platform specific noise will likewise be negligible.

Environmental noise includes ocean wave noise, geomagnetic noise and geologic noise, which components are discussed in respective subsections below.

Ocean Wave Noise. Ocean wave noise originates due to the motion of seawater in the earth's magnetic field. Typical analyses of this effect emphasize the decay of noise intensity with altitude above the ocean surface, where it is concluded that altitudes in the order of 500 feet are sufficient so that other sources of environmental noise dominate.

Figure 3 displays calculated noise power spectra for a stationary sensor at differing depths and wind speeds. The solid curves are constructed from the Pierson-Moskowitz spectrum for long gravity waves in deep water and an empirically derived power transfer function given in reference [a]; the latter pertaining to a sensor depth of 120 feet. Corrections for sensor depth, which are frequency dependent, are made via the theoretical development of reference [b] which is experimentally confirmed in reference [c].

FIGURE 3
CALCULATED OCEAN WAVE NOISE POWER SPECTRA
 (as recorded by a stationary magnetometer)



By way of comparison, a spectrum calculated by different methods by the SSBN Security Program is shown by the dashed curve of Figure 3. There is apparently no reconciliation of the two approaches since the Pierson spectrum for a 30 knot wind speed contains essentially no power at frequencies below .06 Hz. However, when Doppler shift due to vehicle motion is accounted for, the two approaches yield essentially the same power spectrum observed by a moving sensor near the ocean surface. The same would not be true for a subsurface sensor, since low frequency (e.g., $f \leq .04$ Hz) ocean surface noise decays very slowly with depth (and altitude as well).

For a moving sensor the noise spectrum is Doppler shifted. Letting S be the component of sensor speed against the wave motion, power at frequency f is shifted to frequency f' where

$$f' = \left| \frac{S}{2\pi g} f^2 + f \right|$$

and allowing for bandwidth corrections, power (in γ^2/Hz) is multiplied by

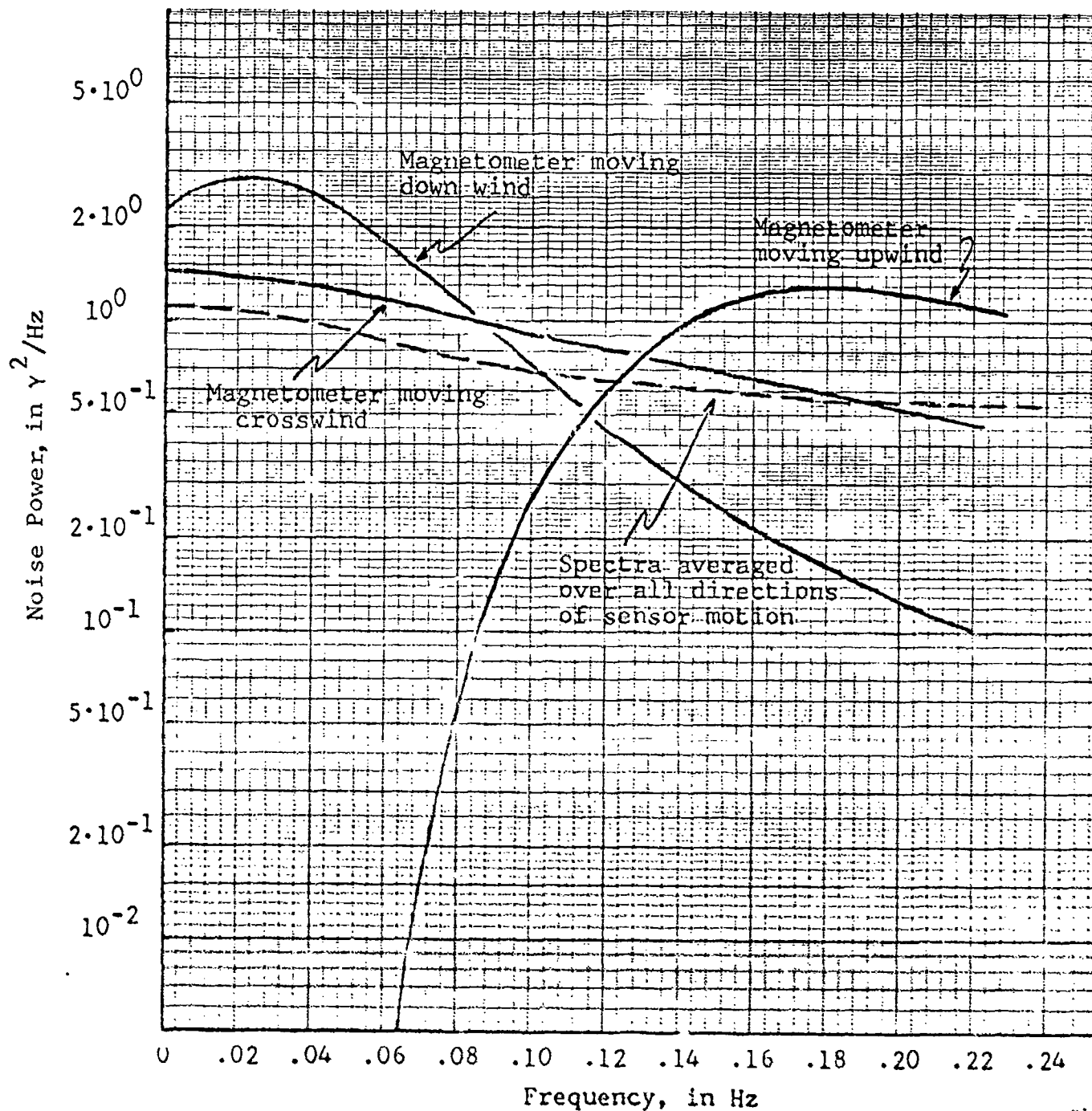
$$(1 + 2Sf/(2\pi g))^{-1}.$$

At this point, the direction of platform motion relative* to the wind (and, hence, expected wave motion) is relevant, and several cases are displayed in Figure 4 for a 60 knot platform speed and

* In constructing the curves of Figure 4, it is assumed that wave amplitude varies as the cosine of the angle between the direction of wave propagation and wind direction, over the angular interval $[-\pi/2, \pi/2]$.

FIGURE 4
CALCULATED OCEAN WAVE NOISE POWER SPECTRA AS RECORDED BY A
MAGNETOMETER AT THE OCEAN SURFACE MOVING AT 60 KNOTS IN 30 KNOT WIND

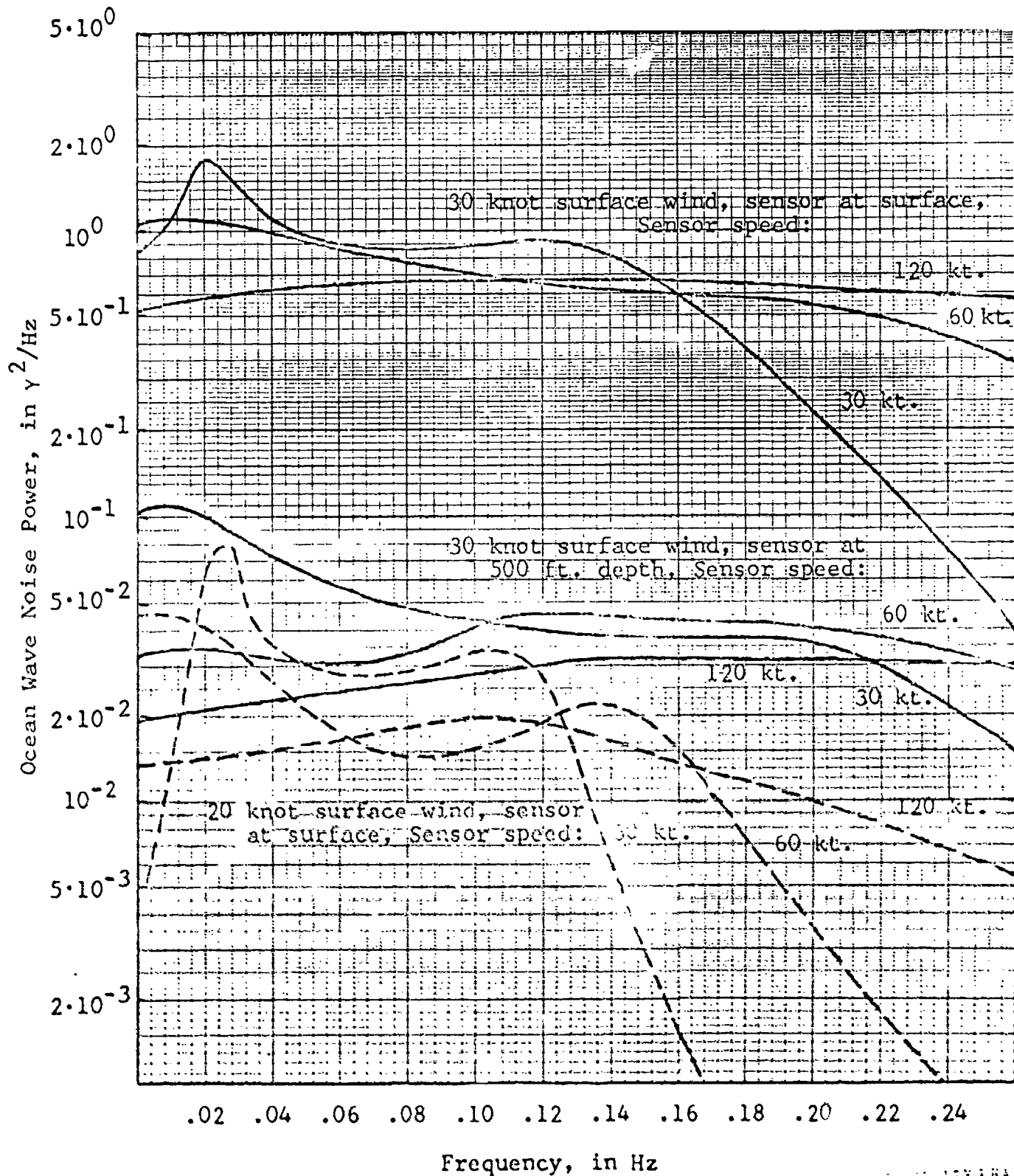
Note: Spectra are calculated from the corresponding curve (30 knot wind, 0 depth) of Figure 3, incorporating Doppler shift as described in the text.



NOT TO BE REPRODUCED
 WITHOUT AUTHORITY

FIGURE 5

CALCULATED OCEAN WAVE NOISE POWER SPECTRA FOR A
SENSOR MOVING AT RANDOM WITH RESPECT TO WAVE MOTION



a 30 knot wind. Except for a vehicle traveling directly into the wind, where all ocean wave power is shifted upwards in frequency, the direction of platform motion is not critical. Again, to avoid a multiplicity of geometric cases, the calculations of this memorandum assume a random orientation between platform and wind (or wave motion) direction. Noise power spectra, Doppler shifted and averaged on this basis, are shown in Figures 4 and 5; the curves of Figure 5 are used in subsequent calculation of detection performance.

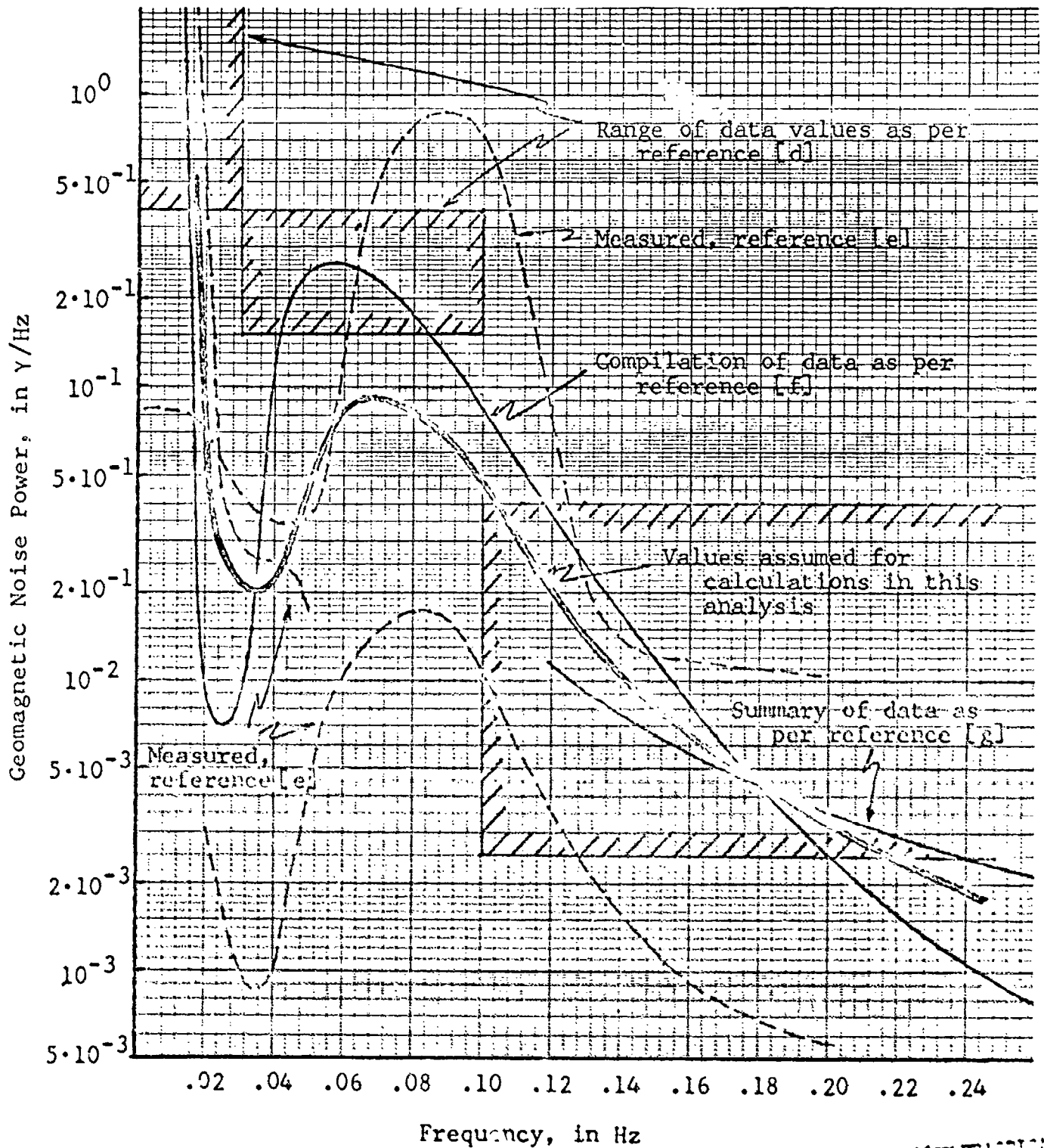
Geomagnetic Noise. Geomagnetic noise consists of temporal variations in the earth's magnetic field, and may be further subdivided into that due to magnetic storm activity (high noise levels occurring about 10% of the time) and micropulsations. Geomagnetic noise is characterized by a high degree of spatial coherence, i.e., lack of variation in the horizontal plane, and is thus unaffected by vehicle speed. Therefore, for present purposes, it suffices to use experimental measurements of geomagnetic noise power, a variety of which are shown in Figure 6. The general dependence on frequency is apparently real although the differing measurements, taken at different locations and times, differ by orders of magnitude.

Calculations of detection performance are based on the subjectively chosen spectrum (γ^2/Hz) indicated in Figure 6. As noted in the summary of results, changes in noise power of a factor of 10, result in changes in calculated detection range by approximately 50%.

Geologic Noise. Geologic noise is due to local magnetic anomalies in the earth's crust, and hence the noise interference at the sensor results from sensor motion through this stationary field.

FIGURE 6

GEOMAGNETIC NOISE POWER SPECTRA
(Measured Values and Compilations of Data)



At the low speeds (and short detection ranges) relevant to the present analysis, the impact of geologic noise is minimal.

A geologic noise power spectrum taken from reference [h] for a "worst" case, i.e., a 180 knot aircraft flying over the mid-Atlantic ridge, is shown in Figure 7. Assuming range and effects are equivalent to those pertaining to a single (target) anomaly, the power spectrum can be translated to other vehicle speeds and water depths by the relation:

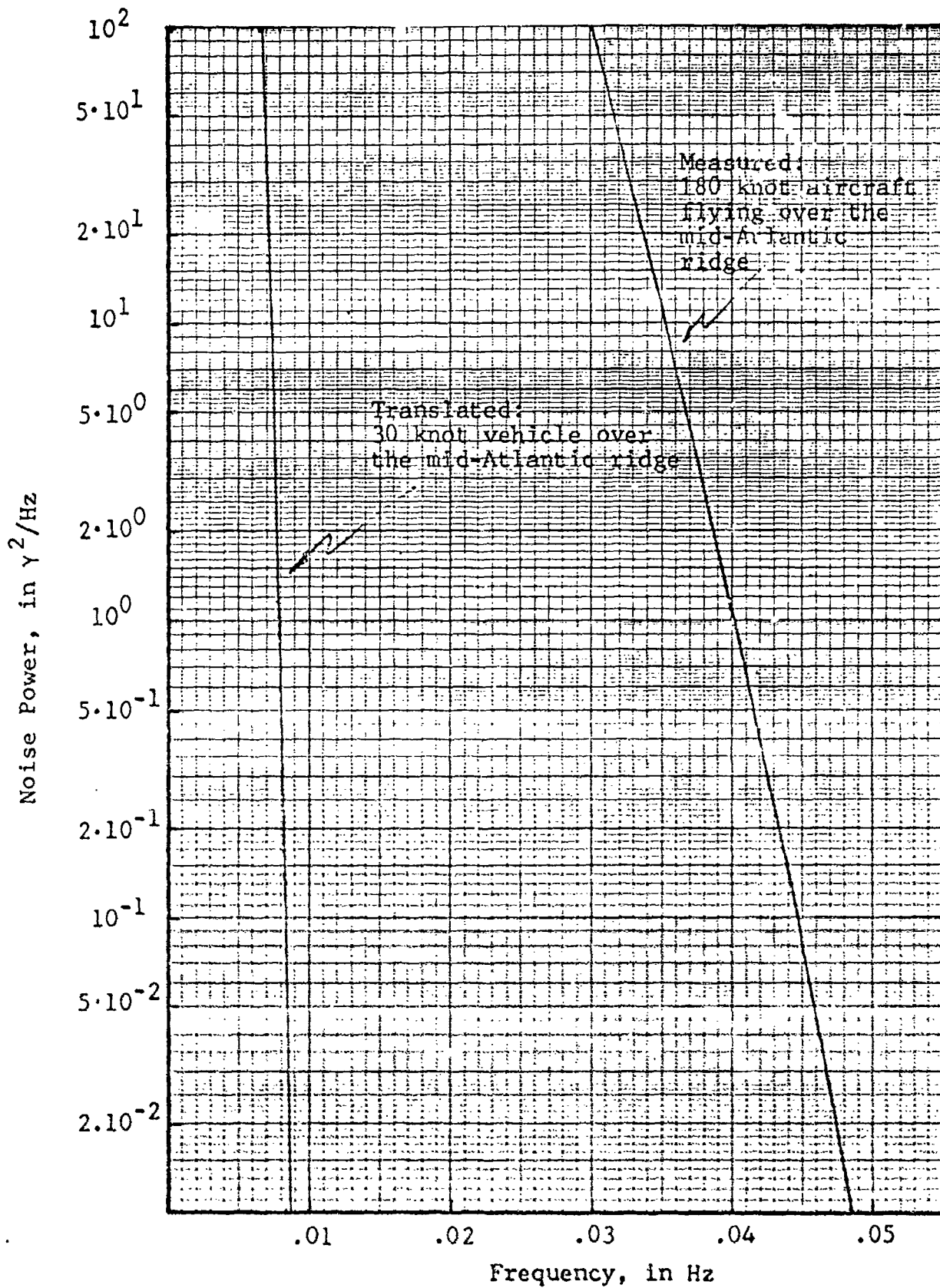
$$\psi_{r_1 V_1}(f) = \frac{V_2^2 r_2^4}{V_1^2 r_1^4} \psi_{r_2 V_2} \left(f \frac{r_1 V_2}{r_2 V_1} \right)$$

where

V_i, r_i = vehicle speed and distance to CPA of the anomaly (here loosely interpreted as ocean depth), and
 $\psi_{rV}(f)$ = the geologic noise power spectrum of a sensor at speed V in water depth r , given in γ^2/Hz .

Figure 7 shows such a translation for a 30 knot platform over the mid-Atlantic ridge; as will be seen subsequently, the noise power is contained in frequencies too low to be of practical interest.

FIGURE 7
GEOLOGIC NOISE POWER SPECTRA



Signal Detection.

The detectability of an anomaly signal is assessed in two ways. First, as is conventional wisdom, it is assumed that the signal is detectable if and only if its observed amplitude is 3 times that of the background noise level. Second, the methods of statistical decision theory are applied to the detection of a (presumed) exactly known signal. If the noise background is Gaussian, this represents optimal performance, and thus yields an upper bound on magnetometer detection capability. Both approaches are illustrated by example calculations in this section.

In the current MAD signal processing system, the magnetometer output is bandpass filtered (in a band expected to contain the temporal variation of the signal) and the output is displayed on a strip chart recorder. In the present analysis, where low platform speeds result in low frequency signals, a significant part of the signal energy must be lost if background noise levels are to be suppressed to reasonable values. Thus, the observed signal amplitude is here estimated by determining the signal energy displayed to the operator and specifying a nominal signal duration, whence signal power and amplitude are determined.

From formula (4), signal energy is given by

$$\text{Signal Energy} = \int_{-\infty}^{\infty} (B_D(t))^2 dt = \frac{m^2}{r_0^6} \int_{-\infty}^{\infty} \left(\sum_{i=1}^3 A_i \psi_i(Vt/r_0) \right)^2 dt$$

and treating the Anderson functions separately, the energy passed through a frequency band $[f, F]$ is given by

$$\text{Observed Signal Energy} = \frac{2m^2}{V^2 r_0^4} \int_{2\pi \underline{f}}^{2\pi \bar{F}} \left(A_i \left| \hat{\phi}_i(wr_0/V) \right| \right)^2 dw, \text{ for } i=1,2,3.$$

Assuming a nominal signal duration of $2r_0/V$, corresponding to $-1 \leq \theta \leq 1$ in Figure 1, the observed signal amplitude is taken to be

$$\text{Observed Signal Amplitude} = \sqrt{2} \left(\frac{m^2}{r_0^6} \int_{2\pi \underline{f}r_0/V}^{2\pi \bar{F}r_0/V} A_i^2 \left| \hat{\phi}_i(\xi) \right|^2 d\xi \right)^{\frac{1}{2}}. \quad (5)$$

(It should be noted that if $\underline{f} = 0$, $\bar{F} \rightarrow \infty$, formula (5) yields values of .92, .35 and .27 for the three Anderson functions, exclusive of coefficient values, whereas the maximal amplitudes are 1.0, .28 and .19 respectively.) Similarly, the observed noise level is calculated by

$$\text{Observed Noise Level} = \sqrt{2} \left(\int_{\underline{f}}^{\bar{F}} \psi(f) df \right)^{\frac{1}{2}}$$

where ψ is a composite noise power spectrum.

Finally then, detection is assumed to occur if and only if

$$\frac{\text{Observed Signal Amplitude}}{\text{Observed Noise Level}} \geq 3$$

or

$$\frac{\frac{m^2}{r_0^6} \int_{2\pi \underline{f}r_0/V}^{2\pi \bar{F}r_0/V} A_i^2 \left| \hat{\phi}_i(\xi) \right|^2 d\xi}{\int_{\underline{f}}^{\bar{F}} \psi(f) df} \geq 9 \quad \text{for } i = 1, 2 \text{ or } 3. \quad (6)$$

In applying inequality (6), \underline{f} is chosen to maximize the left-hand member; the value of \bar{f} is not critical and taken to be .5Hz in all cases.

From a decision theoretic point of view, sensor performance is characterized by a detection index, d (also interpreted as an output signal-to-noise ratio) where, for a matched filter and a known signal:

$$d = \int_{-\infty}^{\infty} \frac{|S(\omega)|^2}{P(\omega)} \frac{d\omega}{2\pi}, \quad (7)$$

where

$S(\omega)$ = the Fourier spectrum of the signal, and

$P(\omega)$ = the power spectral density of the background noise.

Detection index, d , defines an ROC curve by

$$\left[\begin{array}{l} \text{Probability of} \\ \text{detection} \end{array} \right] = \int_{\beta - \sqrt{d}}^{\infty} \frac{1}{\sqrt{2\pi}} \exp\left(-\frac{z^2}{2}\right) dz \quad (8)$$

$$\left[\begin{array}{l} \text{Probability of a} \\ \text{false alarm in a} \\ \text{time interval equal} \\ \text{to the signal duration} \end{array} \right] = \int_{\beta}^{\infty} \frac{1}{\sqrt{2\pi}} \exp\left(-\frac{z^2}{2}\right) dz \quad (9)$$

where β , a detection threshold, varies parametrically from $-\infty$ to $+\infty$. The present analysis assumes a tolerable false alarm rate of .5/hour (one false alarm every two hours), and that the signal is effectively contained in the time interval $[-r_0/V, r_0/V]$, equivalent to $-1 \leq \theta \leq 1$ in Figure 1. Therefore, the detection threshold β is determined by the relationship

$$\left[\begin{array}{l} \text{Tolerable false} \\ \text{alarm rate} \end{array} \right] = \frac{1}{2r_0/v} \int_{\beta}^{\infty} \frac{1}{\sqrt{2\pi}} \exp\left(-\frac{z^2}{2}\right) dz = 0.5/\text{hour}, \quad (10)$$

and thus probability of detection (at CPA equal to r_0) is determined solely by detection index, d .

Returning to formula (7), $|S(w)|$ and $P(w)$ are specified by

$$|S(w)| = \frac{m}{r_0^3} \sum_{i=1}^3 A_i \frac{r_0}{v} \left| \hat{\psi}_i \left(\frac{r_0 w}{v} \right) \right|$$

$$P(w) = \frac{1}{2} \psi \left(\frac{|w|}{2\pi} \right) / 2\pi$$

where $\hat{\psi}_i$ are given by Figure 2, and ψ is the noise power spectrum given by Figures 5 - 7. Substituting the above in formula (7), treating the three Anderson functions separately to avoid peripheral geometric complications, making the change of variables

$$\xi = r_0 w / v$$

and noting that the integrand of (7) is symmetric about $\xi = 0$,

$$d = \frac{4m^2}{r_0^5 v} \int_0^{\infty} \frac{A_i^2 \left| \hat{\psi}_i(\xi) \right|^2}{\psi(\xi v / (2\pi v_0))} d\xi, \text{ for } i = 1, 2 \text{ or } 3. \quad (11)$$

In the above form, it is seen that d decreases as the fifth power of r_0 (in addition to effects due to a change in the relevant noise frequencies) and hence probability of detection varies from .20 to .80 over a very narrow range of CPAs. Thus, it is meaningful to speak of a single detection range, for a particu-

lar geometry represented by the coefficients A_i ; and in this analysis, such a range is taken to be that at which the probability of detection equals 0.50, or

$$\sqrt{d} = \beta.$$

As noted in a previous section, the three Anderson functions comprising the signal are treated separately to avoid a multiplicity of geometric cases; whence, d is taken to be the maximum of the value of formula (11) for $i=1, 2$ or 3 , and $(A_1, A_2, A_3) = (1.0, 1.5, 1.0)$.

Calculation of detection ranges in a particular case is illustrated in the remainder of this section. Figure 8 shows the separate contributions and a composite noise power spectrum for a 60 knot vehicle speed with the sensor towed at 500 feet and 30 knot surface winds. By way of comparison, the spectra of the Anderson functions (with a linear vertical scale) are shown at the bottom of the figure; the horizontal scales are related by:

$$\xi = \frac{2\pi r_0}{V} f$$

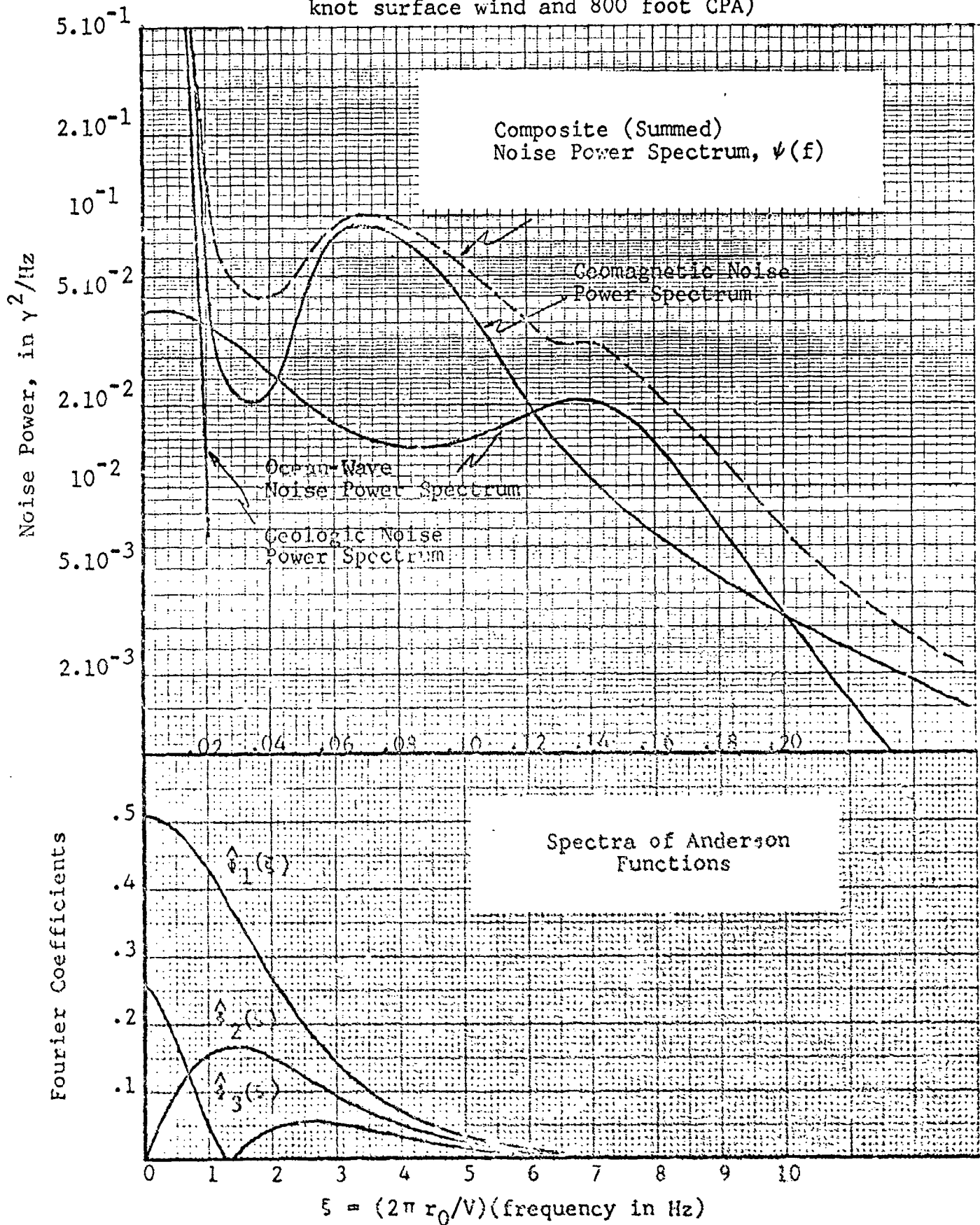
for $r_0 = 800$ feet, $V = 100$ feet/second ≈ 60 knots.

Addressing the first criterion for detection, the integrals of formula (6) are evaluated numerically for the particular case illustrated in Figure 8, with the following results.

FIGURE 8

EXAMPLE NOISE BACKGROUND AND SIGNAL

(60 knot vehicle, 500 foot sensor depth, 30 knot surface wind and 800 foot CPA)



(SIGNAL AMPLITUDE)² / (NOISE LEVEL)²
FOR THE CASE DISPLAYED IN FIGURE 8

Anderson Function			
<u>f</u> , <u>F</u>	i = 1	i = 2	i = 3
.0100, .50	.55	.26	.018
.0125, .50	2.26	1.17	.068
.0150, .50	8.26	4.87	.27
.0175, .50	8.59	5.27	.30
.0200, .50	7.73	5.08	.31

For this case, the optimal low-frequency cut-off is in the order of .015-.0175 Hz and this optimal choice is assumed in assessing detection. (It should be noted that the first and third Anderson functions would be considerably distorted in the output presented to a human operator due to the loss of low frequency and DC components; the resulting reduction in signal amplitude is accommodated by formula (6).)

By the criterion that a signal is detectable if and only if the amplitude is three times the background noise level, the target submarine is not detectable at a CPA of 800 feet.

Similarly, the integral of formula (11) is evaluated numerically with the result that

$$d = 50.1, 33.25, \text{ or } 2.04$$

for $i = 1, 2$ or 3 respectively. Using formula (10) for the tolerable false alarm rate (noting that the units of time are seconds) it is found that for this vehicle speed and CPA,

$$\beta = 2.84.$$

Therefore, for both the first and second Anderson functions,

$\sqrt{d} > \beta$ and the probability of detection, with optimal signal processing, is greater than 0.50; using formula (8) the probability of detection is calculated to be 0.9999, .9984, or .079 for the three Anderson functions respectively.

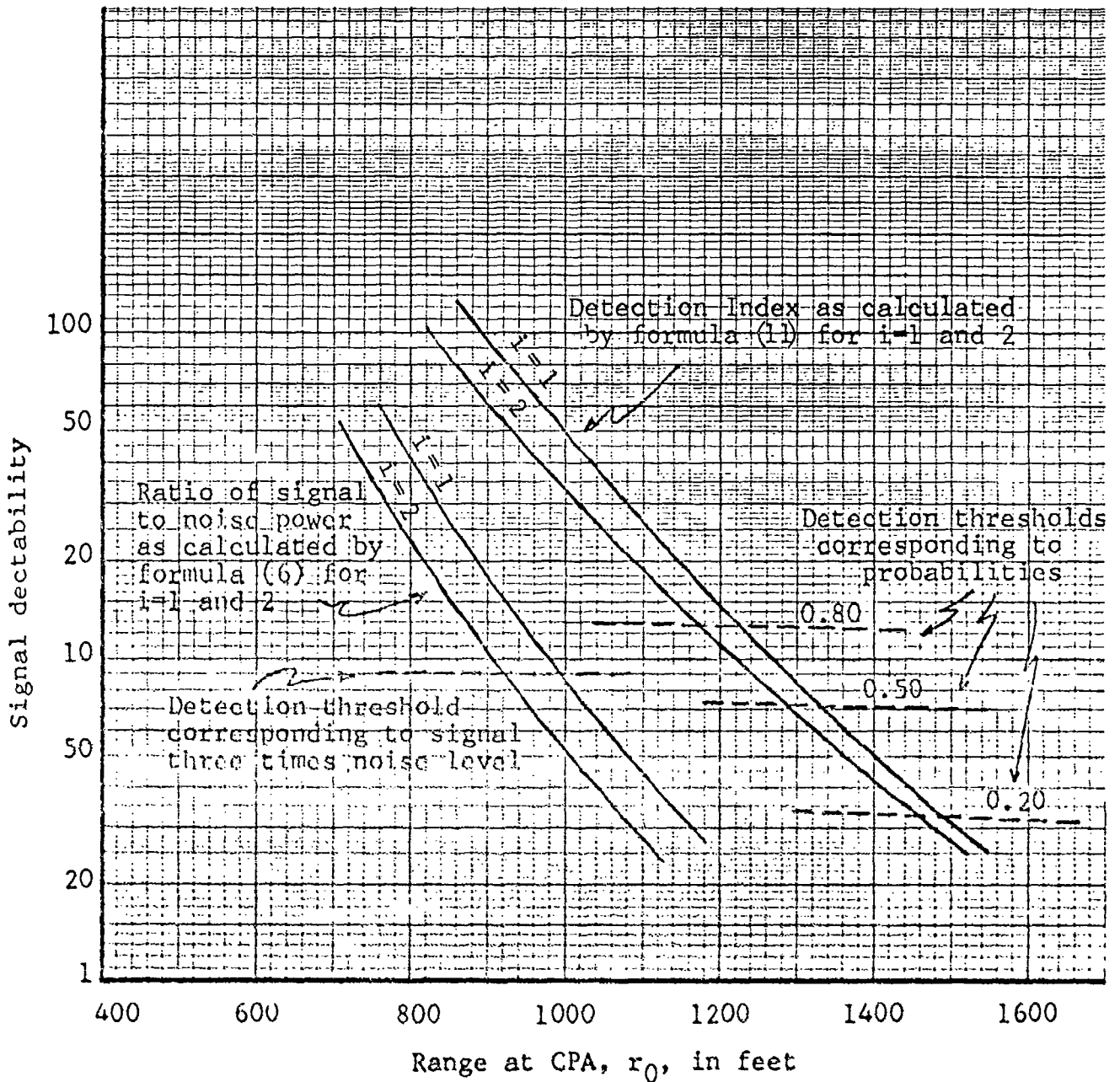
Continuing the example further, the integrals of formulas (6) and (11) are evaluated, numerically, for alternate CPAs, i.e., values of r_0 ; calculated results are shown in Figure 9 along with values of the detection index implying probabilities of detection of 0.20, 0.50 and 0.80. Detection of the third Anderson function is omitted from the figure since such a signal is much less detectable in this noise background (as shown in Figure 8). As stated previously, the maximum detection range resulting from the three Anderson functions treated separately is assumed in the present analysis, whence detection ranges of 990 feet and 1330 feet are obtained from the respective criteria for detection. These values appear in Table 1 for the case of a 60 knot searcher, 500 foot sensor depth and 30 knot wind speed.

Some final points relevant to Figure 9 are noted below. First, signal detectability decreases more rapidly than the inverse sixth or fifth power of range at CPA, from which it follows that changes in signal or noise power by a factor of 10 would change the calculated detection range by less than 50%. This strong range dependence justifies the avoidance of geometric complexities through the treating of each Anderson function separately. The curves of Figure 9 each depend on the square of the Anderson function coefficients, i.e., on A_1^2 , A_2^2 which are separately taken to be 1.0 and 2.25. For an arbitrary encounter geometry, the expected values of A_1^2 , A_2^2 are approximately 0.50 and 1.125 respectively whence almost all encounter geometries will result in a signal detectability comparable to the cases shown. Finally, as previously asserted, probability of detection assuming optimal signal processing varies between 0.80 and 0.20 over a narrow

FIGURE 9

SIGNAL DETECTABILITY vs. CPA

(60 knot searcher, 500 foot sensor depth, 30 knot surface wind)



range interval, here 1220 - 1480 feet. Thus it is meaningful to quote a single, nominal detection range.

Edward P. Loane

Edward P. Loane

References:

- [a] "The Magnetic Fields of Ocean Waves," D. C. Fraser, Geophysics Journal of the Royal Astronomical Society, 11, pp. 507, 1966.
- [b] "Magnetic Variation Associated with Ocean Waves and Swell," J. T. Weaver, Journal of Geophysics Research, 70, pp. 1921, 1965.
- [c] "Magnetic Variations Produced by Ocean Swell," K. C. Maclure, R. A. Hafter, and J. T. Weaver, Nature, 204, pp. 1290, 1964.
- [d] Geomagnetic Gradient Noise Literature Survey, Internal SSBN Security Program Memorandum, by D. Brandt, dated August 27, 1974.
- [e] "Composition of 'Pearls'," K. Vozoff, R.M. Ellis and G. D. Garland, Nature, 194, pp. 539-541, 1962.
- [f] "The Geomagnetic Field," David J. Knecht, Handbook of Geophysics and Space Environments, Air Force Surveys in Geophysics, No. 246, 11.6.4, Revision of Chapter 11, dated September 26, 1972.
- [g] "Magnetometer/Aircraft and Magnetic Gradiometer/Aircraft Threat Element Analysis(U)," by Strategic Systems Department, APL, SSBN Security Program Threat Element Notebook, Vol. 1, POR-3200a, 1976, SECRET.
- [h] ELFE Background Noise, SSBN Security Program Draft Presentation including Visual Aids.